Research Article | Vol. 27, No. 15 | 22 Jul 2019 | OPTICS EXPRESS 21597
Optics EXPRESS

Novel accelerometer realized by a polarization -maintaining photonic crystal fiber for railway monitoring applications

ZHENGYONG LIU,[1,*] LIN HTEIN,[1] DINUSHA SERANDI GUNAWARDENA,[1] WENG-HONG CHUNG,[1] CHAO LU,[2] KANG-KUEN LEE,[1] AND HWA-YAW TAM[1]

[1]*Photonics Research Center, Department of Electrical Engineering, The Hong Kong Polytechnic University, Kowloon, Hong Kong, China*
[2]*Photonics Research Center, Department of Electronic and Information Engineering, The Hong Kong Polytechnic University, Kowloon, Hong Kong, China*
**zhengyong.liu@connect.polyu.hk*

Abstract: In this paper, we present a novel accelerometer based on the Sagnac interferometer configuration using a polarization-maintaining photonic crystal fiber (PM-PCF), which has a sensitivity of ~8 pm/G, and a resonant frequency exceeding 2.5 kHz. The proposed accelerometer is capable of functioning with a constant sensitivity in a large frequency range from 0 to 1 kHz which is much wider than many FBG-based accelerometers. Experimental results obtained from a field test in railway monitoring, demonstrate a broader frequency range for the proposed accelerometer compared to that of the FBG based accelerometer and is comparable to the conventional piezoelectric sensor. The abrupt change in the acceleration measured by the sensor aids in locating any defect or crack present on the railway track. To the best of our knowledge, this is the first demonstration of an accelerometer based on a fiber interferometer aimed for the railway industry. The proposed accelerometer operating at high accelerations (>40 G) and capable of functioning at a broad frequency range, shows significant potential in being used in applications which require detection of strong and fast vibrations, especially in structural health monitoring of trains and railway tracks in real time.

1. Introduction

Since the discovery of photonic crystal fibers (PCFs) in the 1990s [1], they have attracted lots of interest in various applications. Many sensing schemes are proposed based on special structures of air holes that modify the mechanical and optical properties of the fibers compared to standard single mode fibers (SMFs). Owing to the asymmetrical arrangement of the air holes, birefringence can be easily introduced in a PCF which relates to the geometry and internal stress of the fiber. A large number of sensors based on PCFs with high performance have been demonstrated to measure numerous physical parameters, such as strain [1], temperature, pressure [2], lateral force [3], torsion [4], and vibration [5]. Among those, vibration measurements are particularly important in structural health monitoring (SHM), *e.g.* in civil engineering, and condition monitoring in the railway industry [6]. As one of the dynamic measurements, an accelerometer is generally accommodated in characterizing abrupt changes in vibrations. In the recent years, different kinds of accelerometers have been developed incorporating optical fibers consisting of fiber Bragg gratings (FBGs) [7–13] or fiber interferometers (*e.g.* Michelson interferometer [14], Fabry-Pérot interferometer [15]). Compared to the conventional piezoelectric accelerometers, those based on optical fibers are immune to electromagnetic interference (EMI), and possess the capability of being multiplexed in a single strand of fiber. These intrinsic advantages make fiber-optic accelerometers superior in many extreme applications in railway and oil industries. In

#364276 https://doi.org/10.1364/OE.27.021597
Journal © 2019 Received 8 Apr 2019; revised 21 May 2019; accepted 12 Jun 2019; published 17 Jul 2019

Optics EXPRESS

addition, together with the fiber communication technology, it is easier to establish a multifunctional sensing network consisting of all-fiber sensors to monitor acceleration, strain, temperature and other physical parameters such as axle number, train speed etc [16–19], which is ideal for a railway system.

When considering accelerometers based on FBGs, most rely on cantilever-mass [9] or spring-mass mechanisms [12]. The former design typically has an FBG glued onto the cantilever beam, with a mass at the end of the cantilever in order to bend the beam during vibrations. In contrast, the design of a spring-mass or diaphragm-mass system include an FBG which is directly connected to the mass so that the grating can be pulled by the mass while vibrating. Depending on the mechanical designs and the mass used, the sensitivity of such accelerometers can vary from a few pm/G to hundreds of pm/G (G = 9.8 m/s^2) [11,12]. However, the resonant frequency normally varies from ~100 Hz to ~1000 Hz, which limits the operational frequency range with a flat sensitivity to hundreds of Hz [9,12]. Hence, there is a tradeoff between the acceleration sensitivity and the resonant frequency, where the accelerometers with higher sensitivities usually indicate lower resonant peaks. In 2015, Dai *et al* reported a special transducer designed with two symmetrical flexible gemels used to apply a tensile force on the FBG [8]. The advantages of such a design are the high sensitivity (200 pm/G) and the resonant frequency (~3 kHz) that can be achieved. However, the high tendency of fiber breakage and relatively large cross-axis sensitivity affect the overall performance of the system. The FBG based commercially available accelerometers (MOI Model: os7100) exhibit a high shock acceleration of 100 G and a sensitivity of ~16 pm/G, with a resonant frequency limited to only ~700 Hz, which indicates an operational frequency of about 300 Hz [20]. For applications in certain environments, accelerometers functioning at higher resonant frequencies capable of detecting larger accelerations are desirable.

In addition to the FBG-based accelerometers, interferometric configurations are also employed to realize distributed vibration measurements [21]. Most of the distributed vibration sensor systems mainly focus on the localization of the vibration instead of the acceleration characteristics. Since the phase of the interferometer is modulated by vibration, complex demodulated methods are necessary to stabilize the sensing systems. In 2018, Wu *et al* reported a highly sensitive vibration sensor based on a Fabry-Pérot interferometer where vibration frequencies up to 20 kHz were detected due to a flexible FP cavity formed by a silicone elastomer [22]. However, its sensitivity is limited to low acceleration. Recently, in the effort to achieve high performance accelerometers, specialty optical fibers including PCFs [15] have been proposed, providing a new direction for improvement and exploration rather than merely focusing on the mechanical design. Villatoro *et al* in 2017, proposed a strongly coupled multicore fiber to measure vibrations with a very high sensitivity of –4225 pm/N, which may be useful for acoustic measurements [23] even though, high accelerations were not demonstrated. Rong *et al* reported a highly sensitive accelerometer through FBG inscription in a special double-clad fiber consisting of a low-index dip in the center of the fiber core [24]. The accelerometer configuration by bending such a fiber grating, exhibited a high acceleration resolution (1.7×10^{-3} m/s^2, *i.e.* 1.7×10^{-4} G) which is useful in the detection of small accelerations at low frequencies (<100 Hz).

PCFs can be considered as excellent candidates to be employed as novel sensors based on the stress effect, due to the air-hole structures that are introduced in the cross section which offers flexibility in modifying the stress distribution. In this paper, we present a novel accelerometer constructed based on the configuration of a Sagnac interferometer (SI) using a polarization-maintaining PCF (PM-PCF). The PM-PCF is fully embedded between a mass and a substrate. During vibration, the PM-PCF is pressed by the mass periodically, inducing a specific phase change to the interferometer. The principle of this accelerometer is presented and demonstrated using lateral force measurements. It shows a constant sensitivity of ~8 pm/G in a large frequency range up to 1 kHz. The resonant frequency obtained, exceeds 2.5 kHz, resulting in a larger operational frequency range. Since the fiber is directly being pressed

Optics EXPRESS

rather than being pulled by the mass, it is possible to achieve a high acceleration (>40 G). The practicality of this accelerometer is verified by employing it in a field test where the proposed accelerometer was installed in an in-service train. The results obtained are in good agreement with the piezoelectric sensor which was used as a reference and demonstrates a considerably better performance compared to the FBG-based accelerometer. To the best of our knowledge, this is the first fiber accelerometer based on a PM-PCF which demonstrates successful operation in the railway industry. In addition, it will also be beneficial in other extreme applications when monitoring high accelerations in a large frequency range.

2. Fabrication and principle of the SI-based accelerometer

The proposed novel accelerometer is based on a Sagnac interferometer constructed using a PM-PCF (NKT Photonics, PM-1550-01). The PM-PCF was manually spliced to the two branches of a 3-dB coupler, as schematically illustrated in Fig. 1(a). A commercial splicer (Fitel S178) was used to splice PM-PCF to SMF with modified program, following similar procedures as described in [25]. In particular, the arc power and the arc time duration were controlled when splicing. To reduce the collapsing of the air holes in PCF, PM-PCF was positioned and aligned at an offset distance of ~50 µm from the electrodes. Before conducting the repeatable arc discharges, the SMF was pushed towards PM-PCF manually. In this approach, the splicing loss for a single point is <1 dB. The PM-PCF functions as the sensing arm and was coiled into a diameter of ~15 mm. A stainless-steel cylinder mass (56 gram) with a diameter of 25 mm and a height of 15 mm was used to apply a lateral force on the PM-PCF. The 3-dB coupler including the SMFs and PM-PCF as well as the mass were epoxied using Epoxy: EPO-TEK 353ND, ensuring that only the lateral force was applied on the PM-PCF and no other movement existed in the Sagnac loop. The dimensions of the substrate were 65 × 35 × 5 mm, and a suitable cover with a thickness of 2 mm was used to seal the package after the Sagnac interferometer was constructed and then glued to obtain a sufficient fringe visibility (*e.g.* >10 dB). To ensure that the vibration force was applied to one polarization axis of the PM-PCF, the slow axis of the PM-PCF was placed in the same plane, avoiding any possible twist which may occur in the fiber during coiling. To achieve this, the cross sections of both ends of the PCF were checked under the microscope and one side of the fiber was marked along the entire length. During coiling, the marked side was positioned carefully in one plane. The cross sections were checked again after coiling to ensure the placement. Since the lateral force needs to be applied only to a single axis due to the novel design, the cross-axis effect can be ignored.

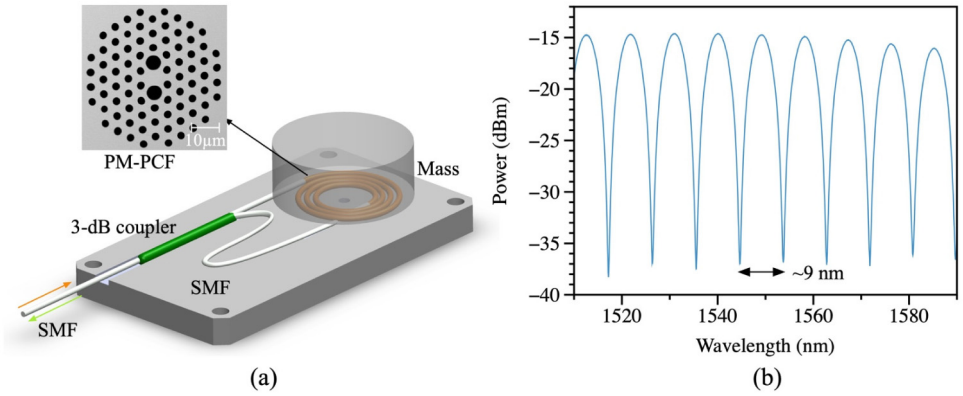

Fig. 1. (a) Schematic figure of the accelerometer based on a Sagnac interferometer using a polarization-maintaining photonic crystal fiber (PM-PCF), and (b) the measured interference spectrum of the sensor using a fiber length of ~0.35 m.

Optics EXPRESS

In principle, when the broadband light is launched from the input end of the 3-dB coupler, it splits into two counter-propagating beams, which interfere constructively or destructively at the same coupler after propagating through the PM-PCF. The reflection spectrum of the SI detected from the input end is expressed by [26]

$$R \cong \frac{1+\cos\delta}{2}, \tag{1}$$

where δ is the phase difference of the two orthogonal modes propagating in the Sagnac loop, which is $(2\pi/\lambda)B \cdot L$. B is the phase birefringence and L is the length of the PM-PCF. Figure 1(b) shows the measured reflection spectrum of the SI using a fiber length of 0.35 m. The fringe spacing obtained is ~9 nm, indicating that the group birefringence (G) of this fiber is $\sim 7.5 \times 10^{-4}$ according to the relationship, $\Delta\lambda = \lambda^2/(G \cdot L)$ [27].

When applying a lateral force on the PM-PCF from one polarized axis, the birefringence changes with respect to the applied force. The relationship between the wavelength change of a trough in the spectrum and the applied force can be formulated as

$$\Delta\lambda = \frac{\lambda}{G(F)}\Delta B(F), \tag{2}$$

where $\Delta\lambda$ is the force-induced spectrum shift, $G(F)$ is the group birefringence after applying a specific force F, and $\Delta B(F)$ is the change of the phase birefringence induced by the force. The simulation was carried out using the COMSOL Multiphysics software. The results indicating a variation in the phase birefringence as a function of the applied lateral force along the fast and slow axes, are plotted in Figs. 2(a) and 2(b), respectively. It can be observed that the birefringence changes linearly with the lateral force, however, based on the orientation of the applied force, follows a different trend. During the experiment, the spectrum shift of such a SI was monitored when applying a lateral force on the PM-PCF via the fast and slow axes. Figures 2(c) and 2(d) demonstrate the relationship between the wavelength of a trough and the lateral force of the fast and slow axes, respectively. The results are consistent with the simulation results according to Eq. (2). The sensitivities of the static force based on the SI configuration are 0.032 nm/N and –0.023 nm/N, respectively for the cases where the lateral forces were applied via the fast and slow axes. The different responses from the fast and slow axes are induced because of the two large air holes, leading to various birefringence changes. Due to the opposite response of these two axes, the orientation of the PM-PCF during coiling is important to maximize the sensitivity of the accelerometer. Hence, the polarization axis of the PM-PCF of the accelerometer needs to be placed in a single plane, with the absence of any twist in the fiber during coiling.

Optics EXPRESS

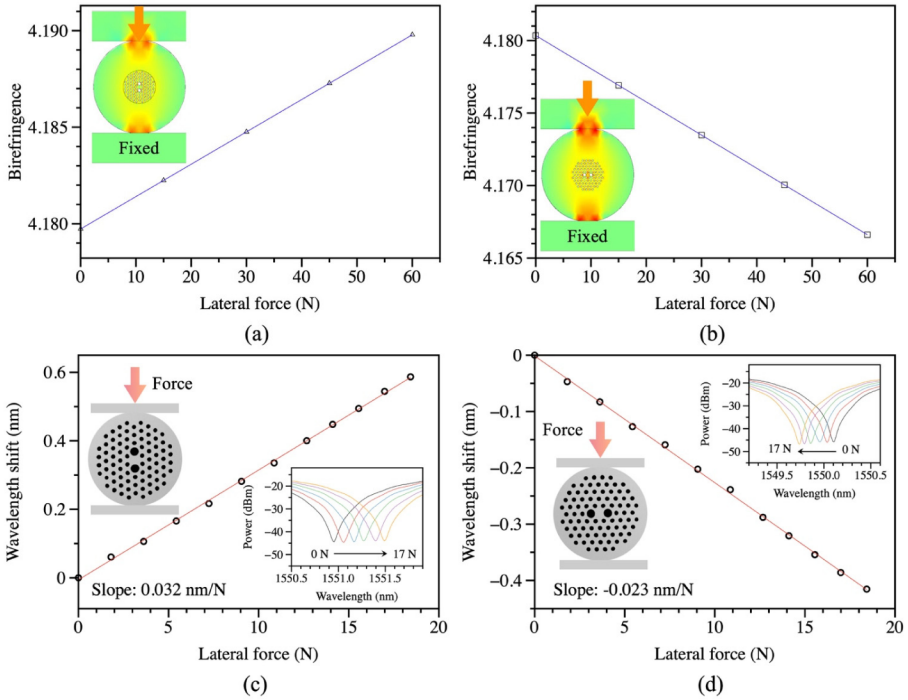

Fig. 2. Simulation results of the phase birefringence of PM-PCF when applying the lateral force along the (a) fast axis and (b) slow axis, and the experimental results of the wavelength shift with respect to the applied force directed towards (c) fast axis and (d) slow axis.

Different from the static lateral force, the accelerometer accounts for the dynamic resonance with a frequency of f and a maximum amplitude of F_m, *i.e.* $F(t) = F_m \cdot \sin(2\pi f t + \varphi_0)$, where t is the vibration time and φ_0 is the initial phase of the resonance. According to $F = \eta ma$, the acceleration has a resonance with the same frequency, where the empirical constant η ($\in [0,1]$) represents the transfer coefficient of the lateral force applied to the fiber after considering the epoxy and coating materials. Typically, $\eta = 1$ means that the vibration-induced force can be fully transferred to the fiber. Taking the relationship between the wavelength shift and the applied force into account (*e.g.* $k = 0.032$ nm/N), the calculated wavelength shift at a specific acceleration ($f = 500$ Hz, $a = 20$ G) is plotted in Fig. 3(a), whereas Fig. 3(b) indicates the corresponding FFT spectrum. As a result, the sensitivity of the accelerometer is estimated to be 35 pm/G ($\eta = 1$) and 10.5 pm/G ($\eta = 0.3$) when the mass is 56 grams.

Optics EXPRESS

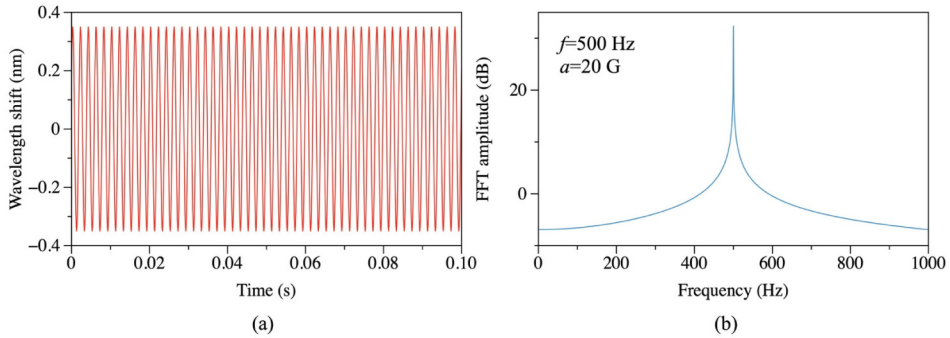

Fig. 3. (a) Calculated wavelength shift of the accelerometer for a vibration of 20 G at a frequency of 500 Hz (η = 1) and (b) the corresponding fast Fourier transform spectrum of the time domain signal.

3. Characterization of the SI-based accelerometer

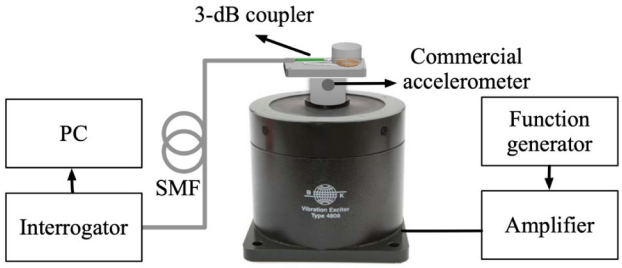

Fig. 4. Experimental setup used to characterize the performance of the proposed accelerometer.

To verify the performance of the aforementioned accelerometer, the vibration tests were conducted using the setup shown in Fig. 4. The SI-based accelerometer was packaged and fixed on a shaker (Bruel & Kjaer: type 4808). A function generator was employed to generate the desired driven signal with a specific frequency, which was then amplified and used to drive the shaker. The actual acceleration applied to the shaker was also calibrated by a commercial accelerometer (Bruel & Kjaer: type 8305) installed underneath the holder. As a result, the wavelength shift induced by the dynamic force during vibration can be calibrated in terms of the actual acceleration. During the experiment, the acceleration of the shaker was increased gradually up to 20 G and the vibration frequency was altered from 50 Hz up to 2500 Hz at a step size of 50 Hz. The wavelength shift of a trough of the spectrum was recorded by an interrogator (MOI model: si155) with a sampling rate of 5 kHz. Figure 5(a) demonstrates the measured results of the wavelength shift in the time domain for the vibrations with maximum accelerations of 8 G, 12 G and 16 G at a frequency of 500 Hz. With different grades of acceleration, the maximum wavelength shift (peak-to-peak) increases with the applied acceleration. By calculating the FFT of the time domain signal, the corresponding vibration frequencies can be obtained. Figure 5(b) shows the results of vibration at frequencies of 100 Hz, 400 Hz, 700 Hz and 1000 Hz. A signal to noise ratio (SNR) of larger than 25 dB is observed with the absence of any harmonic frequencies with increasing acceleration.

Optics EXPRESS

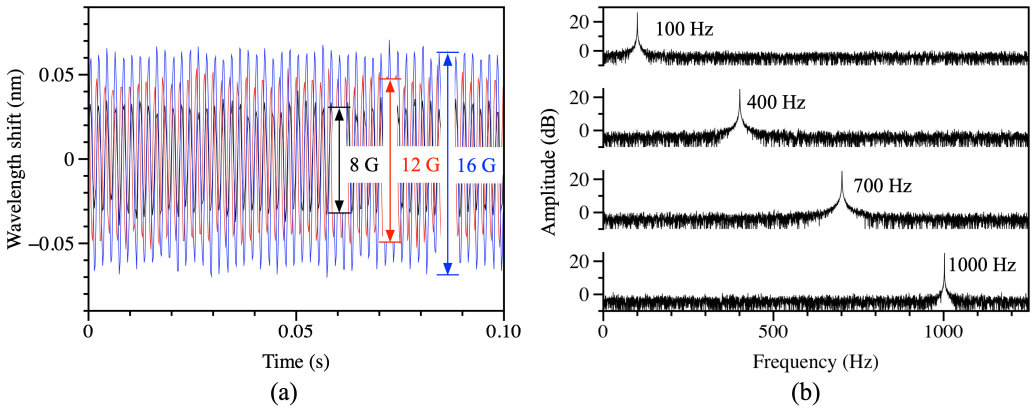

Fig. 5. (a) Experimentally measured wavelength shifts of the accelerometer during vibration at a frequency of 500 Hz and accelerations of 8, 12 and 16 G (b) the fast Fourier transform spectrum of the time-domain signal at frequencies of 100, 400, 700, and 1000 Hz.

Furthermore, the acceleration response was characterized by increasing the acceleration for the frequencies from 0 Hz to 2500 Hz. Figure 6(a) indicates the maximum wavelength shift as a function of the acceleration, when the vibration frequencies range from 100 to 800 Hz. The sensitivities achieved in this frequency range only varies from 7.8 pm/G to 8.5 pm/G (~5% fluctuation), indicating that a stable sensitivity can be obtained at an operational frequency up to 800 Hz. Even at a frequency of 1000 Hz, the sensitivity only amounted to 11.2 pm/G. In comparison, the commercially available FBG based-accelerometer (os7100) from Micro Optics has a resonant frequency of ~700 Hz, and a sensitivity fluctuation of up to 30% when the frequency is over 400 Hz. When the frequency is higher than 1000 Hz, a gradual increase in the sensitivity is observed as shown in Fig. 6(b). The experimentally characterized response is lower than the theoretical estimation (~35 pm/G) due to the acrylate coating and the glue in between the fiber and the mass which acts as an additional buffer. A larger weight of the inertial mass leads to a higher sensitivity but a lower resonant frequency. Therefore, the sensitivity can be further enhanced by using a larger mass. Furthermore, the acrylate coating can be replaced with a polyimide coating to increase the sensitivity as well. With reference to 8 pm/G, the sensitivity (*i.e.*$20 \times \log_{10}(S/S_{ref})$ is within 3 dB, in the frequency range up to 1 kHz which is much broader than a commercial FBG-based accelerometer [20]. The resonant frequency of the proposed SI-based accelerometer is expected to be beyond 2.5 kHz, which was not measured due to the limitation of our setup. As a reference, the actual structure of the accelerometer was modelled and simulated using Solid Mechanics in COMSOL. To simplify the model, only the stainless-steel substrate, mass and one layer of 353ND epoxy (1 mm thickness) were considered. The Young's modulus and Poisson's ratio of stainless steel and epoxy were 195 GPa, 0.29, and 3.56 GPa, 0.4, respectively. As a result, the resonant frequency is estimated to be 3216 Hz (η = 0.3), which is consistent with the experimental estimation (>2.5 kHz). Nevertheless, as a specification, the operational frequency can reach up to 1 kHz without any significant fluctuation in the sensitivity, which is much higher than most FBG-based accelerometers [13,20,28–30], especially those capable of withstanding accelerations higher than 10 G.

Optics EXPRESS

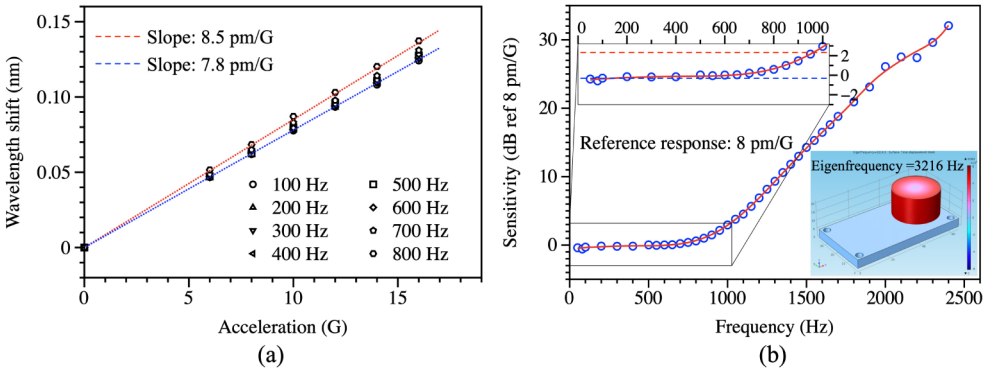

Fig. 6. (a) Measured responses of the accelerometer for a frequency range of 100-800 Hz with sensitivities varying from 7.8 pm/G to 8.5 pm/G, and (b) the measured sensitivity (dB ref 8 pm/G) with respect to the frequency, where the resonant frequency is beyond 2.5 kHz. Inset shows the simulated total displacement at eigenfrequency of 3216 Hz as a reference.

Since the sensing region of the fiber is pressed directly instead of being pulled by the mass, it can withstand high accelerations without any fiber breakage. The maximum acceleration applied during the experiment was ~40 G, which was limited by the shaker, however, no damage was caused to the accelerometer during the process. This is a very important aspect in the railway industry or in any other extreme application where unexpected fast vibrations occasionally occur. The temperature dependence of the SI constructed by PM-PCF with a pure silica core is as low as ~2 pm/°C [31]. After packaging and fixing it with glue, this temperature dependence of the accelerometer was measured to be ~10 pm/°C in another independent experiment, corresponding to a cross-sensitivity of ~1 G. Nevertheless, it is insignificant in practical usage since the accelerometer operates under dynamic vibrations at high frequencies.

4. Field test in railway monitoring

To demonstrate the practical feasibility, the proposed SI-based accelerometer was installed on an in-service train running on a railway line. For comparison and further verification, an FBG-based accelerometer and a piezoelectric accelerometer were installed as well. All these three types of accelerometers were installed on the bogie of one car, and their installation points are illustrated in Fig. 7. The optical signals from the FBG-based and SI-based accelerometers were monitored and recorded using the same interrogator (MOI si155). All the data were collected during the normal operation of the train. Real time monitoring of the vibrations detected by the accelerometers is one of the key parameters used to determine the health condition of the railway track [6].

Optics EXPRESS

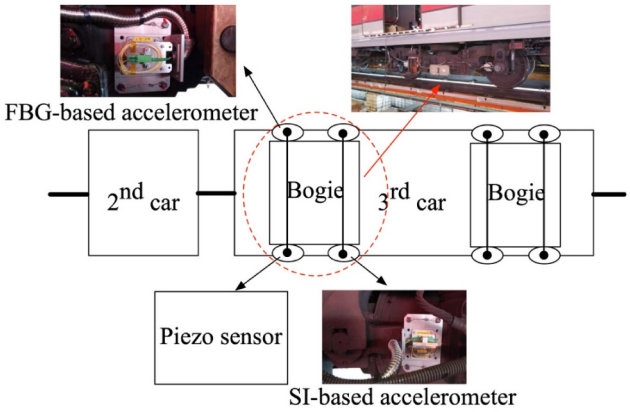

Fig. 7. Schematic figure of the PM-PCF, FBG and piezo based accelerometers installed on the train, insets show the exact location.

Figure 8 demonstrates the results of the acceleration measured by the three sensors when the train travels from station A to station B, where the distance between the two stations were about 1.75 km. From the results, it can be seen that the acceleration measured by the SI-based accelerometer is comparable with the piezo sensor, whereas the FBG-based accelerometer indicates a strong noise level due to its low resonant frequency that is ~250 Hz. The FBG-based accelerometer is homemade, which has a sensitivity and an operation frequency of ~21 pm/G and <50 Hz, respectively. The piezoelectric accelerometer (Dytran Instrument Inc., model: 3333M6T) has a resonant frequency and an operation range of >24 kHz and <10 kHz, respectively. It is expected for the FBG-based accelerometer to have a distorted signal when the vibration frequency is close to its resonant peak, leading to a high noise level. A filter with a cutoff frequency of 250 Hz was used to filter the high frequency resonances of the data measured by the FBG, and the results obtained are plotted in the same figure in red. It is clearly observed from the results, that the acceleration is comparable with those measured by the SI-based and piezoelectric accelerometers. The reason behind the lack of noise at high frequencies in the SI-based accelerometer is its constant response in a much broader frequency range as previously mentioned (Fig. 6). From a practical point of view of vibration monitoring in the railway industry, accelerometers with higher resonant frequencies allow simple data processing to be carried out, improving the decision-making efficiency. It can also measure vibrations at higher frequencies, for example, the resonance exerted by corrugations in the rail track [32]. Typically, defects such as deformations and bending of the railway tracks induce low frequency vibrations (e.g. <100 Hz), which can be identified by the FBG accelerometers. However, minor corrugations or ripples occurring on the railway track generally lead to vibrations of the wheels at high frequencies (e.g. >600-800 Hz), which can be distinguished by accelerometers with high operational frequencies. Thus, more information can be extracted to assess the rail conditions. The SI-based accelerometer can sustain high accelerations and frequencies owing to the novel design of lateral compression, allowing it to detect more defects such as corrugations and ripples on the track.

There is a noteworthy sudden increase in the acceleration (>10 G) at the position of ~128 m that is directly being distinguished by the SI-based as well as piezoelectric accelerometers whereas in the case of FBG-based accelerometer, it is completely hidden in the noise and can be detected only after filtering the high frequency noise. This anomalous signal is caused by a crack on the rail track, which was noticed during regular inspections. Hence, the proposed SI-based accelerometer using a PM-PCF functions commendably in actual field tests and possesses superior characteristics compared to the FBG-based accelerometers.

Optics EXPRESS

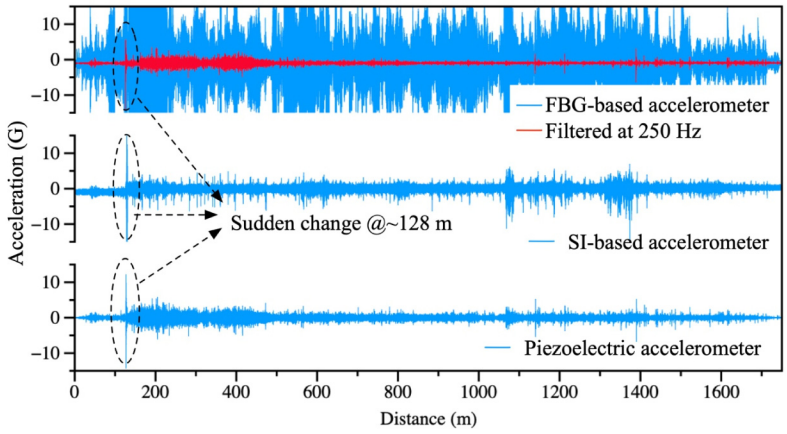

Fig. 8. Measured acceleration using the FBG, PM-PCF and piezo based accelerometers between stations.

5. Conclusion

In conclusion, we have presented a novel fiber accelerometer designed using a PM-PCF in a configuration of a Sagnac interferometer. The proposed accelerometer adopts a design of a "spring-mass", in which the PM-PCF coiled into a small diameter was pressed by the mass, causing an interferometric phase change with respect to the applied vibration. As a result, the response of the acceleration measurement was close to a constant (*i.e.* ~8 pm/G) in a broad frequency range up to 1 kHz. The resonant frequency of the proposed accelerometer is beyond 2.5 kHz. Simulations were carried out to verify the working principle of the proposed accelerometer by applying a lateral force on the PM-PCF. Owing to the novel design, where the PM-PCF was compressed by the mass, the accelerometer can withstand accelerations higher than 40 G, which was limited by the test rig in our lab. To verify the feasibility of the proposed accelerometer, it was installed on an in-service train to monitor the real-time acceleration change during normal operation. The results achieved were comparable with the piezoelectric accelerometer which was also installed for comparison purposes. Additionally, it shows a superior performance in contrast to the FBG-based accelerometer that has a high noise level due to its limited operational frequency range. To the best of our knowledge, this is the first demonstration where a PCF-based accelerometer is employed in railway monitoring. The promising results obtained in the field test make the proposed accelerometer a good candidate for condition monitoring in the railway industry, and can be further incorporated in other fields where monitoring large accelerations at high frequencies is a necessity, especially under the circumstances where EMI is present.

Funding

The Hong Kong Polytechnic University Central Grant projects (1-ZVGB, 1-BBYE, 1-BBYS); National Natural Science Foundation of China (NSFC) (Grant No: 61827820).

References

1. X. Dong, H. Y. Tam, and P. Shum, "Temperature-insensitive strain sensor with polarization-maintaining photonic crystal fiber based Sagnac interferometer," Appl. Phys. Lett. **90**(15), 151113 (2007).
2. W. J. Bock, "High-Pressure Polarimetric Sensor Using Birefringent Optical Fibers," IEEE Trans. Instrum. Meas. **39**(1), 233–237 (1990).
3. P. Zu, C. C. Chan, Y. Jin, Y. Zhang, and X. Dong, "Fabrication of a temperature-insensitive transverse mechanical load sensor by using a photonic crystal fiber-based Sagnac loop," Meas. Sci. Technol. **22**(2), 025204 (2011).
4. F. Zhang, S. Liu, Y. Wang, Y. Huang, X. Xu, C. Fu, T. Wu, C. Liao, and Y. Wang, "Highly sensitive torsion sensor based on directional coupling in twisted photonic crystal fiber," Appl. Phys. Express **11**(4), 042501

Optics EXPRESS

(2018).
5. K. Chah, N. Linze, C. Caucheteur, P. Mégret, P. Tihon, O. Verlinden, S. Sulejmani, T. Geernaert, F. Berghmans, H. Thienpont, and M. Wuilpart, "Temperature-insensitive polarimetric vibration sensor based on HiBi microstructured optical fiber," Appl. Opt. **51**(25), 6130–6138 (2012).
6. H. Y. Tam, S. Y. Liu, S. L. Ho, and T. K. Ho, "Fiber Bragg Grating Sensors for Railway Systems," in *Fiber Bragg Grating Sensors: Recent Advancements, Industrial Applications and Market Exploitation*, A. Cusano and A. Cutolo, eds. (BENTHAM SCIENCE PUBLISHERS, 2012), pp. 197–217.
7. Q. Rong, X. Qiao, T. Guo, W. Bao, D. Su, and H. Yang, "Orientation-dependent fiber-optic accelerometer based on grating inscription over fiber cladding," Opt. Lett. **39**(23), 6616–6619 (2014).
8. Y. Dai, G. Yin, B. Liu, G. Xu, and J. M. Karanja, "Medium-high frequency FBG accelerometer with integrative matrix structure," Appl. Opt. **54**(11), 3115–3121 (2015).
9. N. Basumallick, I. Chatterjee, P. Biswas, K. Dasgupta, and S. Bandyopadhyay, "Fiber Bragg grating accelerometer with enhanced sensitivity," Sens. Actuators A Phys. **173**(1), 108–115 (2012).
10. M. S. Muller, T. C. Buck, and A. W. Koch, "Fiber Bragg grating-based acceleration sensor," in *2009 International Symposium on Optomechatronic Technologies* (IEEE, 2009), pp. 127–132.
11. N. Basumallick, P. Biswas, K. Dasgupta, and S. Bandyopadhyay, "Design optimization of fiber Bragg grating accelerometer for maximum sensitivity," Sens. Actuators A Phys. **194**, 31–39 (2013).
12. J. Wang, Y. Zeng, C. Lin, Z. Hu, G. Peng, and Y. Hu, "A Miniaturized FBG Accelerometer Based on a Thin Polyurethane Shell," IEEE Sens. J. **16**(5), 1210–1216 (2016).
13. Q. P. Liu, X. G. Qiao, J. L. Zhao, Z. A. Jia, H. Gao, and M. Shao, "Novel fiber bragg grating accelerometer based on diaphragm," IEEE Sens. J. **12**(10), 3000–3004 (2012).
14. Y. Duo, H. Xiangge, L. Fei, G. Lijuan, Z. Min, Q. Xiaokang, and Y. Han, "Self-suppression of common-mode noises of the different fiber optic interferometric accelerometers," Opt. Express **26**(12), 15384–15397 (2018).
15. T. Ke, T. Zhu, Y. Rao, and M. Deng, "Accelerometer based on all-fiber Fabry-Pérot interferometer formed by hollow-core photonic crystal fiber," Microw. Opt. Technol. Lett. **52**(11), 2531–2535 (2010).
16. S. Liu, H. Tam, and K. Lee, "Optical fibre networks facilitate shift to predictive maintenance," Int. Railw. J. **57**, 38–40 (2018).
17. S. J. Buggy, S. James, S. Staines, R. Carroll, P. Kitson, D. Farrington, L. Drewett, J. Jaiswal, and R. P. Tatam, "Railway track component condition monitoring using optical fibre Bragg grating sensors," Meas. Sci. Technol. **27**(5), 055201 (2016).
18. D. Kinet, C. Caucheteur, G. Kouroussis, V. Moeyaert, and K. Yüksel, "Railway monitoring system using optical fiber grating accelerometers," Smart Mater. Struct. **27**(10), 105033 (2018).
19. A. Amini, M. Entezami, and M. Papaelias, "Onboard detection of railway axle bearing defects using envelope analysis of high frequency acoustic emission signals," Case Stud. Nondestruct. Test. Eval. **6**, 8–16 (2016).
20. "http://www.micronoptics.com/product/accelerometer-os7100/,".
21. X. Liu, B. Jin, Q. Bai, Y. Wang, D. Wang, and Y. Wang, "Distributed Fiber-Optic Sensors for Vibration Detection," Sensors (Basel) **16**(8), 1164 (2016).
22. S. Wu, L. Wang, X. Chen, and B. Zhou, "Flexible Optical Fiber Fabry-Perot Interferometer based Acoustic and Mechanical Vibration Sensor," J. Lit. Technol. **36**(11), 2216–2221 (2018).
23. J. Villatoro, E. Antonio-Lopez, J. Zubia, A. Schülzgen, and R. Amezcua-Correa, "Interferometer based on strongly coupled multi-core optical fiber for accurate vibration sensing," Opt. Express **25**(21), 25734–25740 (2017).
24. Q. Rong, T. Guo, W. Bao, Z. Shao, G. D. Peng, and X. Qiao, "Highly sensitive fiber-optic accelerometer by grating inscription in specific core dip fiber," Sci. Rep. **7**(1), 11856 (2017).
25. Z. Liu, M.-L. V. Tse, C. Wu, D. Chen, C. Lu, and H.-Y. Tam, "Intermodal coupling of supermodes in a twin-core photonic crystal fiber and its application as a pressure sensor," Opt. Express **20**(19), 21749–21757 (2012).
26. Y. Liu, B. Liu, X. Feng, W. Zhang, G. Zhou, S. Yuan, G. Kai, and X. Dong, "High-birefringence fiber loop mirrors and their applications as sensors," Appl. Opt. **44**(12), 2382–2390 (2005).
27. Z. Liu, H.-Y. Tam, L. Htein, M.-L. V. Tse, and C. Lu, "Microstructured Optical Fiber Sensors," J. Lit. Technol. **35**(16), 3425–3439 (2017).
28. Y. Weng, X. Qiao, T. Guo, M. Hu, Z. Feng, R. Wang, and J. Zhang, "A robust and compact fiber bragg grating vibration sensor for seismic measurement," IEEE Sens. J. **12**(4), 800–804 (2012).
29. K. Li, T. H. T. Chan, M. H. Yau, T. Nguyen, D. P. Thambiratnam, and H. Y. Tam, "Very sensitive fiber Bragg grating accelerometer using transverse forces with an easy over-range protection and low cross axial sensitivity," Appl. Opt. **52**(25), 6401–6410 (2013).
30. J. Wang, G. Peng, Z. Hu, H. Yang, and Y. Hu, "Design and analysis of a high sensitivity FBG accelerometer based on local strain amplification," IEEE Sens. J. **15**(10), 5442–5449 (2015).
31. H. Y. Fu, H. Y. Tam, L.-Y. Shao, X. Dong, P. K. A. Wai, C. Lu, and S. K. Khijwania, "Pressure sensor realized with polarization-maintaining photonic crystal fiber-based Sagnac interferometer," Appl. Opt. **47**(15), 2835–2839 (2008).
32. S. L. Grassie, "Characteristics, causes, and treatments," Proc. Inst. Mech. Eng. Part F J. Rail Rapid Transit **223**(6), 581–596 (2009).